INTERNATIONAL JOURNAL FOR NUMERICAL METHODS IN ENGINEERING
Int. J. Numer. Meth. Engng 2010; **82**:157–183
Published online 15 October 2009 in Wiley InterScience (www.interscience.wiley.com). DOI: 10.1002/nme.2761

Hybrid domain decomposition algorithms for compressible and almost incompressible elasticity

Clark R. Dohrmann[1,*,†] and Olof B. Widlund[2]

[1]*Sandia National Laboratories, Mail Stop 0346, Albuquerque, NM 87185-0346, U.S.A.*
[2]*Courant Institute, 251 Mercer Street, New York, NY 10012, U.S.A.*

SUMMARY

Overlapping Schwarz methods are considered for mixed finite element approximations of linear elasticity, with discontinuous pressure spaces, as well as for compressible elasticity approximated by standard conforming finite elements. The coarse components of the preconditioners are based on spaces, with a number of degrees of freedom per subdomain which are uniformly bounded, which are similar to those previously developed for scalar elliptic problems and domain decomposition methods of iterative substructuring type, i.e. methods based on nonoverlapping decompositions of the domain. The local components of the new preconditioners are based on solvers on a set of overlapping subdomains.

In the current study, the dimension of the coarse spaces is smaller than in recently developed algorithms; in the compressible case all independent face degrees of freedom have been eliminated while in the almost incompressible case five out of six are not needed. In many cases, this will result in a reduction of the dimension of the coarse space by about one half compared with that of the algorithm previously considered. In addition, in spite of using overlapping subdomains to define the local components of the preconditioner, values of the residual and the approximate solution need only to be retained on the interface between the subdomains in the iteration of the new hybrid Schwarz algorithm. The use of discontinuous pressures makes it possible to work exclusively with symmetric, positive-definite problems and the standard preconditioned conjugate gradient method.

Bounds are established for the condition number of the preconditioned operators. The bound for the almost incompressible case grows in proportion to the square of the logarithm of the number of degrees of freedom of individual subdomains and the third power of the relative overlap between the overlapping subdomains, and it is independent of the Poisson ratio as well as jumps in the Lamé parameters across the interface between the subdomains. Numerical results illustrate the findings. Copyright © 2009 John Wiley & Sons, Ltd.

Received 7 January 2009; Revised 25 June 2009; Accepted 28 August 2009

*Correspondence to: Clark R. Dohrmann, Sandia National Laboratories, Mail Stop 0346, Albuquerque, NM 87185-0346, U.S.A.
†E-mail: crdohrm@sandia.gov

Contract/grant sponsor: The United States Department of Energy's National Nuclear Security Administration; contract/grant number: DE-AC04-94AL85000
Contract/grant sponsor: U.S. Department of Energy; contract/grant number: DE-FG02-06ER25718
Contract/grant sponsor: National Science Foundation; contract/grant number: DMS-0513251

KEY WORDS: domain decomposition; overlapping Schwarz; preconditioners; iterative methods; almost incompressible elasticity; mixed finite element methods

1. INTRODUCTION

We recently considered overlapping Schwarz algorithms for almost incompressible elasticity problems in [1]. Earlier theory for overlapping Schwarz methods for elasticity was restricted to the compressible case in which the Poisson ratio ν is bounded away from its maximum value of $\frac{1}{2}$; see [2, Section 8]. A relatively rich coarse space was used in our recent study, which effectively accommodates all positive values of $\nu<\frac{1}{2}$. It is an extension of a component of iterative substructuring methods developed about 15 years ago for scalar elliptic problems; see [3] and also [2, Algorithm 5.16]. These domain decomposition methods are hybrids in that they borrow components of the preconditioners from two main families of algorithms; see [2, Chapters 3 and 5]. Recent applications of such extended coarse spaces to a variety of different problem types appear in [4], and similar algorithms have already been used successfully as part of a production-level iterative solver in the parallel structural dynamics code Salinas [5].

In this study, we will only consider problems in three dimensions. In that case, the coarse space of our recent study uses three degrees of freedom for each subdomain vertex, five or six for each subdomain edge, and six degrees of freedom for each subdomain face. In this paper, we will show that almost equally strong results can be obtained after switching to a coarse space with only one independent degree of freedom for each subdomain face and that, in fact, all of them can be eliminated in the compressible case. We will also demonstrate that the overlapping subdomains and a particular type of hybrid Schwarz method, which together with the coarse space define the preconditioner, can be chosen so that the residuals and iterates need only to be retained on the interface of the partitioning of the domain into subdomains. In this respect, our algorithms resemble early work by Barry Smith, see [6, 7] and [2, Algorithm 5.5]. We note that his algorithm uses a conventional finite element space on a coarse triangulation of the domain for the coarse component of the preconditioner.

In our analysis, we can focus on our new coarse spaces while the estimates for the local contributions to the preconditioner require fewer new arguments; we can borrow much of what is needed from our recent paper, in particular, from [1, Section 5.3]. We also note that, as in [1], our approach does not require access to individual subdomain matrices, i.e. we can work directly with a globally assembled matrix; this can be an advantage in finite element practice.

An early application of overlapping Schwarz methods to mixed formulations of linear elasticity and incompressible Stokes problems is given in [8]. In that work, the coarse spaces were based on the same mixed finite element methods on coarse meshes and both continuous and discontinuous pressure spaces were considered. An analysis of these methods was not provided, but their performance was shown to be quite competitive with block diagonal and block triangular preconditioners, see [9].

Related iterative substructuring methods as in [2, Chapter 6], for incompressible or almost incompressible problems appear in [10–13]. For each of these methods, special care is required to ensure that the coarse space is properly constructed. As a result, standard coarse spaces for compressible problems must be modified and enriched to accommodate incompressible or almost incompressible cases.

DOI: 10.1002/nme

In this paper, we again restrict our attention to finite elements with discontinuous pressure interpolation. By doing so, it is possible to eliminate the pressure unknowns at the element level. As the assembled matrix is symmetric and positive definite, an important consequence is that the same solution algorithm, as for compressible elasticity, can be used for the almost incompressible case and that the method of preconditioned conjugate gradients can then be used to accelerate the iteration.

The remainder of this paper is organized as follows. In Section 2, we review the equations of linear elasticity, focusing on the almost incompressible case. We also introduce mixed finite element approximations and then describe the algorithms, discuss their parallel implementation, and formulate the main results in Section 3. These results are proven in Section 4; the remainder of the paper can also be read independently and that section can therefore be bypassed. Results of numerical experiments are given in Section 5.

2. ELASTICITY AND MIXED AND STANDARD FINITE ELEMENTS

Let $\Omega \subset \mathbb{R}^3$ be a domain and let $\partial\Omega_D$ be a nonempty subset of its boundary $\partial\Omega$ and introduce the Sobolev space $\mathbf{V} := \{\mathbf{v} \in \mathbf{H}^1(\Omega) : \mathbf{v}|_{\partial\Omega_D} = 0\}$. Here $\mathbf{H}^1(\Omega) := H^1(\Omega)^3$. The linear elasticity problem consists in finding the displacement $\mathbf{u} \in \mathbf{V}$ of the domain Ω, fixed along $\partial\Omega_D$, subject to a surface force of density $\mathbf{g}$, along $\partial\Omega_N = \partial\Omega \setminus \partial\Omega_D$, and a body force $\mathbf{f}$:

$$2\int_\Omega \mu\varepsilon(\mathbf{u}) : \varepsilon(\mathbf{v})\,\mathrm{d}x + \int_\Omega \lambda \operatorname{div} u \operatorname{div} v\,\mathrm{d}x = \langle \mathbf{F}, \mathbf{v}\rangle \quad \forall \mathbf{v} \in \mathbf{V} \tag{1}$$

Here $\lambda(x)$ and $\mu(x)$ are the Lamé parameters, $\varepsilon_{ij}(\mathbf{u}) = \frac{1}{2}(\partial u_i/\partial x_j + \partial u_j/\partial x_i)$ the linearized strain tensor, and two inner products are defined by

$$\varepsilon(\mathbf{u}) : \varepsilon(\mathbf{v}) = \sum_{i=1}^{3}\sum_{j=1}^{3} \varepsilon_{ij}(\mathbf{u})\varepsilon_{ij}(\mathbf{v}), \quad \langle \mathbf{F}, \mathbf{v}\rangle = \int_\Omega \sum_{i=1}^{3} f_i v_i\,\mathrm{d}x + \int_{\partial\Omega_N} \sum_{i=1}^{3} g_i v_i\,\mathrm{d}A$$

The Lamé parameters can be expressed in terms of the Poisson ratio v and Young's modulus E:

$$\lambda = \frac{Ev}{(1+v)(1-2v)}, \quad \mu = \frac{E}{2(1+v)}$$

The domain Ω is partitioned into nonoverlapping subdomains Ω_i. We assume, for simplicity, that the Lamé parameters are constant in each subdomain. As our analysis will be carried out for one subdomain at a time, we can then work with problems with constant coefficients. The bound for the condition number of our algorithm will be independent of the values of all these parameters.

2.1. A saddle-point formulation

In the compressible case, we can use standard finite element approximations. However, when the material becomes almost incompressible, the Poisson ratio v approaches the value $\frac{1}{2}$ and $\lambda/\mu = 2v/(1-2v)$ approaches infinity. In such cases, finite element discretizations of this pure

DOI: 10.1002/nme

displacement formulation will increasingly suffer from locking and very slow convergence of the finite element solution.

A well-known remedy is based on introducing the new variable $p = -\lambda \operatorname{div} u \in U \subset L^2(\Omega)$ that we will call pressure, and replacing the pure displacement problem (1) with a mixed formulation: find $(\mathbf{u}, p) \in \mathbf{V} \times U$ such that

$$\begin{aligned} &\int_\Omega \mu \varepsilon(\mathbf{u}) : \varepsilon(\mathbf{v}) \, \mathrm{d}x - \int_\Omega \operatorname{div} v p \, \mathrm{d}x = <\mathbf{F}, \mathbf{v}> \quad \forall \mathbf{v} \in \mathbf{V} \\ &- \int_\Omega \operatorname{div} u q \, \mathrm{d}x - \int_\Omega 1/\lambda p q \, \mathrm{d}x = 0 \quad \forall q \in U \end{aligned} \tag{2}$$

see Brezzi and Fortin [14] or Brenner and Scott [15].

In the case of homogeneous Dirichlet boundary conditions for $\mathbf{u}$ on all of $\partial\Omega$, we will choose $U := L_0^2(\Omega) := \{q \in L^2(\Omega) : \int_\Omega q \, \mathrm{d}x = 0\}$, as it follows from the divergence theorem that the pressure will have a zero mean value. For nonzero Dirichlet boundary data, the same is true if the net flux satisfies $\int_{\partial\Omega} \mathbf{u} \cdot \mathbf{n} \, \mathrm{d}s = 0$, where $\mathbf{n}$ is the outward normal. If, on the other hand, the boundary conditions are mixed (part essential and part natural), then there is always a unique solution with a pressure component in $U = L^2(\Omega)$. Rather than discussing two somewhat different cases, we will, from now on, focus on the case with homogeneous Dirichlet boundary conditions on all of $\partial\Omega$.

The net fluxes $\int_{\partial\widetilde{\Omega}} \mathbf{u} \cdot \mathbf{n} \, \mathrm{d}A$, across the boundary $\partial\widetilde{\Omega}$, of subsets $\widetilde{\Omega}$ of individual subdomains, will be important in our analysis; see Lemma 3. Only if they vanish, are there divergence-free extensions of the boundary values for which the bilinear form $\int_{\widetilde{\Omega}} \lambda \operatorname{div} u \operatorname{div} v \, \mathrm{d}x$ will then vanish.

In our analysis, we will work only with the restrictions of Equations (2) to individual subdomains Ω_i, or subsets of such subdomains. In such cases, we can factor out the constants μ_i and $1/\lambda_i$ and we will use the notation $a_i(\mathbf{u}, \mathbf{v})$, $b_i(\mathbf{v}, p)$, and $c_i(p, q)$ for the three resulting bilinear forms associated with the subdomain Ω_i.

In the absence of essential boundary conditions, the elasticity operator has zero energy modes, which are the rigid body modes. There are six of them; they are given in Section 3.

By letting $\lambda_i/\mu_i \to \infty$, we obtain the limiting problem for incompressible linear elasticity and also a formulation of the Stokes system for incompressible fluids. A penalty term, as in the compressible case, could also originate from stabilization techniques or penalty formulations for the Stokes problems.

A Korn inequality for the subspace orthogonal to the rigid body modes establishes an equivalence between the square of the semi-norm in $\mathbf{H}^1(\Omega_i)$ and the bilinear form

$$a_i(\mathbf{u}, \mathbf{u}) = 2 \int_{\Omega_i} \varepsilon(\mathbf{u}) : \varepsilon(\mathbf{u}) \, \mathrm{d}x$$

see further Lemma 4. This will make it possible to use many tools and results developed in the studies of scalar elliptic problems. We will work with the scaled $\mathbf{H}^1(\Omega_i)$-norm defined by

$$\|\mathbf{u}\|^2_{\mathbf{H}^1(\Omega_i)} := |\mathbf{u}|^2_{\mathbf{H}^1(\Omega_i)} + (1/H_i^2) \|\mathbf{u}\|^2_{\mathbf{L}^2(\Omega_i)}$$

where H_i is the diameter of the subdomain Ω_i.

DOI: 10.1002/nme

2.2. *Mixed finite element methods with discontinuous pressures*

We assume that the domain Ω is decomposed into N nonoverlapping subdomains Ω_i. The interface of this decomposition is given by

$$\Gamma := \left(\bigcup_{i=1}^{N} \partial\Omega_i \right) \Big\backslash \partial\Omega$$

To simplify the discussion, we will assume, as in [2, Assumption 4.3], that each subdomain is the union of shape-regular tetrahedral elements of a global conforming coarse mesh and that the number of such tetrahedra forming any individual subdomain is uniformly bounded. We note that this assumption makes the subdomains shape regular, i.e. they have bounded aspect ratios. This assumption makes it possible to use technical tools developed in [2, Section 4.6] in the analysis. Each subdomain is further partitioned into many shape-regular elements. We assume that the nodes match across the interface between the subdomains and we denote the set of elements by $\mathscr{T}_h$. We note that recent advances in the analysis of domain decomposition methods defined on quite irregular subdomains would allow us to extend all our results, in the case of two dimensions, to very irregular subdomains that are only *John domains*; see [1, Section 6] and [16, 17].

In our experimental work, we have chosen to work primarily with the $Q_2(h) - P_1(h)$ finite elements: the displacement space is $\mathbf{V}^h := (Q_2(h))^3$ (continuous tri-quadratics), while the pressure space consists of discontinuous, piecewise linear functions:

$$U^h := \{q \in U : q|_T \in P_1(T) \ \forall T \in \mathscr{T}_h\}$$

The two spaces are defined on the same hexahedral mesh. This mixed finite element method satisfies a uniform inf–sup condition:

$$\sup_{\mathbf{v}\in\mathbf{V}^h} \frac{b_i(\mathbf{v}, q)}{a_i(\mathbf{v}, \mathbf{v})^{1/2}} \geqslant \beta c_i(q, q)^{1/2} \quad \forall q \in U_i^h \cap L_0^2(\Omega_i), \quad \beta > 0 \tag{3}$$

There are optimal $O(h^2)$ error estimates for both displacements and pressures for this mixed finite element method provided that unmapped linear functions are used for the pressure space; see Boffi and Gastaldi [18]. The parameter β depends on the domain and, in particular, it varies inversely with the aspect ratio of the domain; these matters are discussed at length in [1, Sections 5.2 and 5.3]. This is the origin of two of three factors of H/δ in our condition number bound in the almost incompressible case; see Theorem 1.

We note that while finite element methods based on hexahedra and quadrilaterals enjoy popularity, our theory applies equally well to any stable mixed method, e.g. one based on tetrahedral elements, as long as the pressure space is discontinuous.

In matrix form, the mixed finite element approximation of (2) for subdomain Ω_i will contribute to the stiffness matrix

$$\begin{bmatrix} \mu_i A^{(i)} & B^{(i)T} \\ B^{(i)} & (-1/\lambda_i) C^{(i)} \end{bmatrix} \tag{4}$$

Given that the pressure approximation is discontinuous, we can write the matrix $C^{(i)}$ in block diagonal form with the size of the blocks equal to the number of pressure degrees of freedom in an individual element. Therefore, at the expense of solving a few small linear systems of equations

DOI: 10.1002/nme

for each element, we can eliminate the pressure unknowns and obtain a reduced, positive-definite, symmetric subdomain matrix

$$\widetilde{A}^{(i)} = \mu_i A^{(i)} + \lambda_i B^{(i)\mathrm{T}} C^{(i)-1} B^{(i)} \tag{5}$$

Just as in the compressible case, these submatrices can be assembled into $\widetilde{A}$, which represents the energy of the entire system. The corresponding bilinear forms are denoted by $\widetilde{a}_i(\cdot,\cdot)$ and $\widetilde{a}(\cdot,\cdot)$.

3. THE ALGORITHM AND THE MAIN RESULTS

We will describe and analyze our algorithm as a two-level Schwarz method, as in [2, Chapters 2, 3, and 5], defined in terms of a set of subspaces. We focus on the more complicated almost incompressible case; the compressible case needs only to be discussed briefly. In the almost incompressible case, we will work with the displacement variables only and the positive-definite formulation (5) obtained after all pressure degrees of freedom have been eliminated.

3.1. The subspaces of the Schwarz algorithm

We will use a smaller coarse space $\mathbf{V}_0$ than in our recent study [1], and a pair of local spaces $\mathbf{V}_i$ and $\mathbf{V}_{i\delta}$ associated with each subdomain Ω_i.

As the subdomains, which define the local components of the overlapping Schwarz preconditioner, we will use the nonoverlapping subdomains Ω_i into which the given domain Ω has been divided. We note that the Dirichlet solvers on these subdomains, which are needed to compute local corrections, are also used to compute the coarse basis functions of our algorithm from their boundary values. Additionally, we will also use *boundary layer* subdomains $\Omega_{i\delta}$ constructed as the union of layers of elements on both sides of the local interface $\Gamma_i := \partial\Omega_i \cap \Gamma$; see Figure 1, right, for a three-dimensional picture. Each of these subdomains is characterized by a parameter δ_i, which is the distance from Γ_i to $\partial\Omega_{i\delta} \setminus \partial\Omega$. We note that for a small overlap, δ_i, the factorization of the stiffness matrices for the $\Omega_{i\delta}$ can be considerably less expensive than that for the subdomain Ω_i.

We note that the domain decomposition preconditioners of *interface-strip* type have been considered in [19, 20]. The global components of these preconditioners are obtained from solvers of problems defined on the union of all the $\Omega_{i\delta}$ and they therefore differ from ours.

We build the local components of our Schwarz preconditioner by restricting the original problem to the subdomains Ω_i and $\Omega_{i\delta}$, in the customary way, and by solving Dirichlet problems with zero boundary data to obtain the related local corrections.

All elements of the coarse space are discrete saddle-point harmonic functions in the sense that they are minimal energy extensions of values given on the interface; in the almost incompressible case they can be computed by solving Dirichlet problems for each Ω_i, using matrices obtained from $\widetilde{A}^{(i)}$.

Definition 1
The discrete saddle-point harmonic function for boundary data w_Γ has the vector representation

$$w_{\mathrm{sh}} = \begin{bmatrix} w_I \\ w_\Gamma \end{bmatrix}$$

DOI: 10.1002/nme

where

$$\widetilde{A}_{II}^{(i)} w_I^{(i)} = -\widetilde{A}_{I\Gamma}^{(i)} w_\Gamma^{(i)}$$

Here, $\widetilde{A}_{II}^{(i)}$ is a leading principal minor of $\widetilde{A}^{(i)}$, if the interior variables are all ordered ahead of those of the interface, $\widetilde{A}_{I\Gamma}^{(i)}$ represents the coupling between the interface and the interior of the subdomain Ω_i, etc.

To introduce the coarse space $\mathbf{V}_0$, we first decompose the local interfaces Γ_i into faces $\mathscr{F}^{ij}$, edges $\mathscr{E}^{ik}$, and vertices $\mathscr{V}^{i\ell}$. A face is an open subset of Γ_i and an edge is an open subset of the boundaries of several faces. A node on $\mathscr{F}^{ij}$ is common to the boundaries of two subdomains Ω_i and Ω_j, while those on an edge typically are common to more than two. The vertices are endpoints of the edges. For an additional discussion of how to define these sets, even for very irregular subdomains, see [21–23].

The smaller coarse component space is similar to that of the algorithm studied in [1]. In turn, it was adapted from older iterative substructuring algorithms described in [2, Section 5.4] and first developed for scalar elliptic problems in [3]. Because of the larger null space of the elasticity operator, the coarse space must be enriched to make it work for elasticity; see [2, Sections 8.3 and 8.4]. This is related to the well-known null space property, which is necessary to obtain scalability, i.e. a bound on the convergence, which does not depend on the number of subdomains; see the discussion in [24, 25].

The rigid body modes are three translations

$$\mathbf{r}_1 := \begin{bmatrix} 1 \\ 0 \\ 0 \end{bmatrix}, \quad \mathbf{r}_2 := \begin{bmatrix} 0 \\ 1 \\ 0 \end{bmatrix}, \quad \mathbf{r}_3 := \begin{bmatrix} 0 \\ 0 \\ 1 \end{bmatrix} \tag{6}$$

and three rotations

$$\mathbf{r}_4 := \frac{1}{H_i} \begin{bmatrix} 0 \\ -x_3 + \hat{x}_3 \\ x_2 - \hat{x}_2 \end{bmatrix}, \quad \mathbf{r}_5 := \frac{1}{H_i} \begin{bmatrix} x_3 - \hat{x}_3 \\ 0 \\ -x_1 + \hat{x}_1 \end{bmatrix}, \quad \mathbf{r}_6 := \frac{1}{H_i} \begin{bmatrix} -x_2 + \hat{x}_2 \\ x_1 - \hat{x}_1 \\ 0 \end{bmatrix} \tag{7}$$

where $\hat{x} \in \Omega_i$ can be chosen as a midpoint of an edge or face. The shift of the origin makes this basis for the space of rigid body modes well conditioned, and the scaling and shift make these six functions scale in the same way with H_i. This ensures that norms of the six functions are comparable.

We will now recall the coarse basis functions of our previous algorithm. Linear combinations of them will then be used to define the basis functions for the smaller coarse space of the new algorithm.

The coarse basis functions for the algorithm in [1] can be defined by using cutoff functions $\theta_{\mathscr{F}^{ij}}, \theta_{\mathscr{E}^{ik}}$, and $\theta_{\mathscr{V}^{i\ell}}$. The face function $\theta_{\mathscr{F}^{ij}}$ equals 1 at all the nodes of the face and vanishes at all other nodes on the interface. The edge functions $\theta_{\mathscr{E}^{ik}}$ and vertex functions $\theta_{\mathscr{V}^{i\ell}}$ are defined similarly.

For each face, we can use the finite element interpolant of the product of this face cutoff function and the rigid body modes to obtain six linearly independent functions $I^h(\theta_{\mathscr{F}^{ij}} \mathbf{r}_k)$; we extend the

DOI: 10.1002/nme

resulting boundary values into the interior of the subdomains as discrete saddle-point harmonic functions. Here, I^h is the interpolation operator, which maps onto the finite element space $\mathbf{V}^h$. The boundary values for these functions, which are all used as coarse basis functions in [1], can also be obtained by restricting the rigid body modes to the nodes of $\mathcal{F}^{ij}$ and setting the values at all other interface nodes to zero.

Similarly, for a straight subdomain edge, we obtain five linearly independent rigid body modes since, as is easy to see, a rigid body mode representing a rotation, with the edge as its axis, is invisible on the edge; for a detailed discussion on the case of curved edges, for which we use six degrees of freedom, see [22]. In [1], we thus use coarse basis functions associated with the edge, which are given on Γ by $I^h(\theta_{\mathcal{E}^{ik}}\mathbf{r})$ where $\mathbf{r}\in\mathcal{RB}$.

For each vertex, finally, we have three degrees of freedom representing the displacement at that point.

We will now modify this coarse space and eliminate most of the independent face coarse degrees of freedom. The construction is inspired by earlier work on wire basket-based methods and in particular by Pavarino and Widlund [26], which in turn builds on [27, 28]; see also [2, 222–223]. We will use modified coarse basis functions $\theta^m_{\mathcal{E}^{ik}}$ and $\theta^m_{\mathcal{V}^{i\ell}}$ associated with subdomain edges and vertices, respectively, and with a specific rigid body mode $\mathbf{r}_m$. For each such subdomain edge and vertex, there will be contributions given in terms of the face functions described above for each face with a boundary that contains the edge or vertex in question.

Thus, we obtain the modified edge coarse basis function $\theta^m_{\mathcal{E}^{ik}}$ by extending its values to the faces that have this edge in common. Let us consider one face $\mathcal{F}^{ij}$, one edge $\mathcal{E}^{ik}\subset\partial\mathcal{F}^{ij}$, and one rigid body mode $\mathbf{r}_m$, which define one of the edge coarse basis functions given above.

The face contributions to this modified edge function are of the form

$$\sum_{n=1}^{6}\alpha^{ik}_{nm}I^h(\theta_{\mathcal{F}^{ij}}\mathbf{r}_n)$$

To determine the coefficients α^{ik}_{nm}, for the modified edge coarse basis function $\theta^m_{\mathcal{E}^{ik}}$, we solve a linear least-squares problem:

$$\min_{\alpha^{ik}_{nm}}\left\|I^h(\theta_{\mathcal{E}^{ik}}\mathbf{r}_m)-\sum_{n=1}^{6}\alpha^{ik}_{nm}\mathbf{r}_n\right\|^2_{\mathbf{L}^2(\partial\mathcal{F}^{ij})}$$

Here, $\mathbf{L}^2(\partial\mathcal{F}^{ij})=L^2(\partial\mathcal{F}^{ij})^3$.

Since the rigid body modes are linearly independent and all of order 1, it is easy to see that the matrix of the normal equations is well conditioned and that all its elements are of order H_i. The elements on the right-hand side are also of order H_i being defined by integrals of functions of order 1 over the edge, which has a length of order H_i. Therefore all the α^{ik}_{nm} will be uniformly bounded.

The modification of the subdomain vertex coarse basis functions, by adding the same type of face contributions, proceeds similarly by solving least-squares problems. There are two differences. There are only three such functions for each vertex and in the least-squares problem $I^h(\theta_{\mathcal{E}^{ik}}\mathbf{r}_m)$ is replaced by $I^h(\theta_{\mathcal{V}^{i\ell}}\mathbf{r}_m), m=1,2,3$. While the matrix of the normal equations remains the same, the components on the right-hand side will be of the order h_i as the vertex functions vanish at all but one node on Γ.

DOI: 10.1002/nme

We have thus established the following result:

Lemma 1
The coefficients α_{nm} of the modified coarse edge basis function $\theta^m_{\mathscr{E}^{ik}}$ are all $O(1)$ and those of the modified coarse vertex basis functions $\theta^m_{\mathscr{V}^{i\ell}}$ are all $O(h_i/H_i)$.

We use these estimates and the following bounds:

$$|I^h(\theta_{\mathscr{F}^{ij}}\mathbf{r}_k)|^2_{\mathbf{H}^1(\Omega_i)} \leqslant C(1+\log(H_i/h_i))H_i, \quad k=1,\ldots,6 \tag{8}$$

which are obtained by a small modification of the proof of [2, Lemma 4.25]. (We use the fact that the rigid body modes $\mathbf{r}_k$ have components that are linear functions, which are uniformly bounded with gradients bounded by C/H_i.) In addition, we use the fact that

$$|I^h(\theta_{\mathscr{E}^{ik}}\mathbf{r}_m)|^2_{\mathbf{H}^1(\Omega_i)} \leqslant C H_i \tag{9}$$

and

$$|I^h(\theta_{\mathscr{V}^{i\ell}}\mathbf{r}_m)|^2_{\mathbf{H}^1(\Omega_i)} \leqslant C h_i \tag{10}$$

These are elementary bounds obtained by estimating the energy of the trivial extensions of these functions. We find:

Lemma 2
The modified coarse edge basis function $\theta^m_{\mathscr{E}^{ik}}$ satisfies

$$|\theta^m_{\mathscr{E}^{ik}}|^2_{\mathbf{H}^1(\Omega_i)} \leqslant C(1+\log(H_i/h_i))H_i$$

and

$$\|\theta^m_{\mathscr{E}^{ik}}\|^2_{\mathbf{L}^2(\mathscr{F}^{ij})} \leqslant C H_i^2$$

The modified coarse vertex basis function $\theta^m_{\mathscr{V}^{i\ell}}$ satisfies

$$|\theta^m_{\mathscr{V}^{i\ell}}|^2_{\mathbf{H}^1(\Omega_i)} \leqslant C(1+\log(H_i/h_i))h_i$$

and

$$\|\theta^m_{\mathscr{V}^{i\ell}}\|^2_{\mathbf{L}^2(\mathscr{F}^{ij})} \leqslant C h_i H_i$$

We note that the energy of these modified basis functions exceeds those of the original edge and vertex functions by a factor $(1+\log(H/h))$; cf. (9) and (10).

It is clear from our construction that, when restricted to an interior subdomain, this coarse space will contain all the rigid body modes. As previously noted, this is a requirement for obtaining a scalable algorithm; see, e.g. [2, Section 8.2].

We note that in practice we can find good weights, $\alpha_{\ell m}$, to define the extension of the edge and vertex coarse basis functions to the interior nodes of the face, by replacing the $\mathbf{L}^2$-norm over the boundary of the face by an ℓ^2-norm over the values at the nodes of the same set. Lemmas 1 and 2 are still valid.

DOI: 10.1002/nme

We have now constructed a complete coarse space for the compressible case. For the almost incompressible case, we will add one independent coarse basis function for each face. For a flat face, we choose a *face bubble function* $\theta_{\mathscr{F}^{ij}}\mathbf{n}_{\mathscr{F}^{ij}}$ where $\mathbf{n}_{\mathscr{F}^{ij}}$ is a unit normal to the face. We note that this function is linearly independent of the edge and vertex basis functions as it vanishes on the entire boundary of the face while the modified edge and vertex functions do not.

We can also define a suitable average normal direction for a curved face by first constructing a matrix with three columns and where each row contains the three coordinates of a node on $\mathscr{F}^{ij}$. We then shift the origin of the coordinate system so that the average of the elements of each of the columns vanishes. By computing the singular value decomposition $U\Sigma V^{\mathrm{T}}$ of this matrix, we will, in particular, find the orthogonal matrix V of order 3. Its third column, the right singular vector associated with the smallest singular value, will be our choice. It is the normal to the plane through the origin, after the shift, for which the sum of the squares of the distance of the nodes on the curved face to the plane is minimized. We note that this construction, related to *principal component analysis*, has been known since 1901; see [29].

3.2. A hybrid Schwarz algorithm

We also need to specify the Schwarz method used. We note that [2, Chapter 2] provides an introduction to the abstract theory of Schwarz methods. We will recall the definition of the projections from which a Schwarz method is built; for simplicity, we will assume that exact solvers are used for the local problems defined on the overlapping subdomains as well as for the global, coarse problem. We also recall that $\widetilde{a}(\cdot,\cdot)$ is the displacement-only bilinear form for the entire domain Ω and that $\widetilde{a}_i(\cdot,\cdot)$ is that for the subdomain Ω_i. We also use $\widetilde{a}_{i\delta}(\cdot,\cdot)$ obtained similarly for the boundary layer subdomain $\Omega_{i\delta}$.

For any $i \geqslant 1$, we use an extension operator $R_i^{\mathrm{T}}: \mathbf{V}_i \rightarrow \mathbf{V}^h$; this is a simple extension by zero to the nodes not in Ω_i. Extension operators $R_{i\delta}^{\mathrm{T}}$ are defined similarly and R_0^{T} imbeds $\mathbf{V}_0$ into $\mathbf{V}^h$.

Associated with the coarse space is a projection $P_0: \mathbf{V}^h \rightarrow \mathbf{V}_0$; it is orthogonal with respect to the $\widetilde{a}(\cdot,\cdot)$-inner product. For the local spaces $\mathbf{V}_i$ and $\mathbf{V}_{i\delta}$, there are projections $P_i: \mathbf{V}^h \rightarrow R_i^{\mathrm{T}}\mathbf{V}_i$ and $P_{i\delta}: \mathbf{V}^h \rightarrow R_{i\delta}^{\mathrm{T}}\mathbf{V}_{i\delta}$ defined by

$$P_i = R_i^{\mathrm{T}}\widetilde{P}_i \quad \text{with } \widetilde{P}_i \text{ defined by } \widetilde{a}_i(\widetilde{P}_i\mathbf{u}, \mathbf{v}) = \widetilde{a}(\mathbf{u}, R_i^{\mathrm{T}}\mathbf{v}) \quad \forall \mathbf{v} \in \mathbf{V}_i$$

and

$$P_{i\delta} = R_{i\delta}^{\mathrm{T}}\widetilde{P}_{i\delta} \quad \text{with } \widetilde{P}_{i\delta} \text{ defined by } \widetilde{a}_{i\delta}(\widetilde{P}_{i\delta}\mathbf{u}, \mathbf{v}) = \widetilde{a}(\mathbf{u}, R_{i\delta}^{\mathrm{T}}\mathbf{v}) \quad \forall \mathbf{v} \in \mathbf{V}_{i\delta}$$

In this study, we use a Schwarz method of hybrid type; cf. [2, Section 2.5.2]. An early example of such a hybrid method is the Neumann–Neumann algorithm as described in [30] and [2, Section 6.2]. In that algorithm, a coarse space correction is computed in the first and third of three fractional steps, while the rest of the corrections are handled as in an additive Schwarz method. Here, we will instead consider the Schwarz method based on the polynomial

$$P_{\mathrm{hyb}} := \left(I - \sum_{i=1}^{N} P_i\right)\left(P_0 + \sum_{i=1}^{N} P_{i\delta}\right)\left(I - \sum_{i=1}^{N} P_i\right) \tag{11}$$

We note that this hybrid Schwarz polynomial, together with the full specification of the coarse and local spaces, fully define our domain decomposition algorithm. See, Section 3.3 for a discussion on some implementation details.

DOI: 10.1002/nme

Just as in the case discussed in [2, Section 2.5.2], the first factor is a projection; this follows from the observations that the P_i are projections and that as Ω_i and Ω_j do not intersect $P_i P_j = 0, i \neq j$. The application of the third (and first) factor of (11) eliminates all residuals interior to the subdomains Ω_i resulting in piecewise discrete saddle-point harmonic functions and thus fully defined by their values on the interface Γ. By eliminating all residuals in the interior of the subdomains initially, all the residuals of the conjugate gradient iteration can be made discrete saddle-point harmonic. We also note that from the second iteration on, we only need to apply the projection $(I - \sum_{i=1}^{N} P_i)$ once in each step of the iteration.

The main effort in deriving a bound for the condition number of the operator P_{hyb} is to provide an estimate of the parameter C_0^2 in a decomposition lemma

$$\widetilde{a}(\mathbf{u}_0, \mathbf{u}_0) + \sum_{i=1}^{N} \widetilde{a}_i(\mathbf{u}_i, \mathbf{u}_i) + \sum_{i=1}^{N} \widetilde{a}_{i\delta}(\mathbf{u}_{i\delta}, \mathbf{u}_{i\delta}) \leqslant C_0^2 \widetilde{a}(\mathbf{u}, \mathbf{u}) \quad \forall \mathbf{u} \in \mathbf{V}^h \tag{12}$$

for some choice of $\{\mathbf{u}_i\}_0^N, \mathbf{u}_i \in \mathbf{V}_i$ and $\{\mathbf{u}_{i\delta}\}_1^N, \mathbf{u}_{i\delta} \in \mathbf{V}_{i\delta}$, such that

$$\mathbf{u} = \sum_{i=0}^{N} R_i^{\mathrm{T}} \mathbf{u}_i + \sum_{i=1}^{N} R_{i\delta}^{\mathrm{T}} \mathbf{u}_{i\delta} \tag{13}$$

cf. the standard Schwarz theory, as developed in [2, Section 2.3]. A lower bound on C_0^{-2} provides a lower bound for the additive Schwarz operator, based on these subspaces; see [2, Lemma 2.5]. It is also known and easy to show that the lower bound of P_{hyb} is at least as good as that of the additive method; see [31] or [2, Lemma 2.15].

An upper bound on the norm of $P_0 + \sum_1^N P_{i\delta}$ is obtained by a standard coloring argument as in [2, Section 2.5.1]. As the first and third factors of P_{hyb} are projections, they do not contribute to the bound of the norm of our hybrid Schwarz operator. Thus, we obtain a constant upper bound for P_{hyb} and an upper bound for the condition number of P_{hyb} in terms of an upper bound for C_0^2.

Our main result, obtained by estimating C_0^2, is:

Theorem 1 (*Almost incompressible elasticity*)
The condition number of our domain decomposition method, which uses one independent face coarse degree of freedom for each face of Γ, satisfies

$$\kappa(P_{\text{hyb}}) \leqslant C(H/\delta)^3(1 + \log(H/h))^2$$

Here C is a constant that is independent of the number of subdomains and their diameters, the mesh size, and the values of the Lamé parameters. It depends only on the shape regularity of the elements and the subdomains.

As in many domain decomposition results, H/h is shorthand for $\max_i(H_i/h_i)$, where h_i is the smallest diameter of the elements of Ω_i. Similarly, H/δ is the largest ratio of H_i and δ_i.

Remark 1
This result is weaker than the main result in [1] in that we have a factor $(1 + \log(H/h))^2$ instead of $(1 + \log(H/\delta))(1 + \log(H/h))$. The origin of this loss is the bound of the coarse component $\mathbf{u}_0$ associated with the subdomain edges; see (20) and (22). Our experiments indicate that the bound of Theorem 1 is not sharp while those in [1] are. In particular, the three powers of (H/δ) in the main theorems of both papers cannot be improved.

DOI: 10.1002/nme

We also have a result for the compressible case:

Theorem 2 (*Compressible elasticity*)
The condition number of our domain decomposition method, without any independent coarse face degrees of freedom, satisfies

$$\kappa(P_{\text{hyb}}) \leqslant C(H/\delta)(1+\log(H/h))^2$$

Here C is a constant, independent of the number of subdomains and their diameters and the mesh size. It depends only on the shape regularity of the elements and the subdomains and the Poisson ratios v_i.

3.3. Implementation of the Schwarz algorithm

We recall that $\widetilde{A}^{(i)}$ denotes the stiffness matrix and let f_i be the load vector for Ω_i after that all pressure degrees of freedom have been eliminated. The vector of unknowns for the closure of Ω_i is given by $R_i x$, where each row of R_i has a single nonzero entry of unity and x is the global vector of unknowns. The assembled stiffness matrix $\widetilde{A}$ and load vector f are then given by

$$\widetilde{A} = \sum_{i=1}^{N} R_i^{\mathrm{T}} \widetilde{A}^{(i)} R_i, \quad f = \sum_{i=1}^{N} R_i^{\mathrm{T}} f_i$$

A vector in the coarse space can be expressed as $R_0^{\mathrm{T}} q$, where R_0^{T} is the coarse space matrix and q is a vector of coarse degrees of freedom. Columns of the matrix R_0^{T} can be obtained as described earlier in this section. Let R_{iI}, $R_{i\Gamma}$, and $R_{i\delta}$ select the components of x for the interior of Ω_i, the boundary of Ω_i, and the interior of the boundary layer region $\Omega_{i\delta}$, respectively, and define

$$\widetilde{A}_{II}^{(i)} = R_{iI} \widetilde{A} R_{iI}^{\mathrm{T}}, \quad \widetilde{A}^{(i\delta)} = R_{i\delta} \widetilde{A} R_{i\delta}^{\mathrm{T}}$$

Given the linear system $\widetilde{A}x = f$, the first step is to calculate an initial approximation x_0 and residual r_0,

$$x_0 = \sum_{i=1}^{N} R_{iI}^{\mathrm{T}} \widetilde{A}_{II}^{(i)-1} R_{iI} f, \quad r_0 = f - \widetilde{A} x_0$$

We can verify that $R_{i\Gamma} x_0 = 0$ and $R_{iI} r_0 = 0$ for $i = 1, \ldots, N$, i.e. x_0 vanishes on all subdomain boundaries and r_0 is zero in each subdomain interior.

The linear system $\widetilde{A}y = r_0$ can be solved iteratively using preconditioned conjugate gradients given that $\widetilde{A}$ is symmetric and positive definite. Once y is obtained, the solution of the original linear system is given by $x_0 + y$.

The action of our preconditioner on a residual vector r is calculated as follows:

1. Calculate the local boundary layer correction $z_1 = \sum_{i=1}^{N} R_{i\delta}^{\mathrm{T}} \widetilde{A}^{(i\delta)-1} R_{i\delta} r$.
2. Calculate the coarse correction $z_2 = R_0^{\mathrm{T}} (R_0 \widetilde{A} R_0^{\mathrm{T}})^{-1} R_0 r$.
3. Update the residual $\tilde{r} = r - \widetilde{A}(z_1 + z_2)$ and calculate a static condensation correction $z_3 = \sum_{i=1}^{N} R_{iI}^{\mathrm{T}} \widetilde{A}_{II}^{(i)-1} R_{iI} \tilde{r}$.
4. Calculate the preconditioned residual $z = z_1 + z_2 + z_3$.

DOI: 10.1002/nme

As $R_{iI}r=0$, the static condensation correction in Step 3 ensures that the preconditioned residual z satisfies $R_{iI}\widetilde{A}z=0$. Accordingly, we only need to store residuals on subdomain interfaces during the conjugate gradient iterations. This is true for the other vectors used in the conjugate gradient iterations as well. Steps 1 and 3 can be done easily in parallel, but Step 2 may not. If the coarse problem size becomes too large, then approximate solutions for Step 2 can be obtained by applying a preconditioner for the coarse correction matrix, similar to the one described here.

4. PROOFS OF THE MAIN RESULTS

We first note that for the case of the richer coarse space considered in [1], there is little new to prove in case we use the subdomains $\Omega_{i\delta}$ and the original subdomains Ω_i to define the local components of the preconditioner; see further Section 4.2. We will, therefore, focus on the effects of the smaller coarse space and derive an interpolation formula onto that space based on the discussion and results of Section 3.1. In our proofs, we will use that the length of each subdomain edge is bounded from below by cH_i and that the area of each subdomain face by cH_i^2, where c is a positive constant; these bounds follow from the assumptions made on our subdomains.

As in the theory for iterative substructuring algorithms, see [2, Chapters 4, 5, and 6], the analysis can be carried out for one subdomain Ω_i only and variations in the values of the Lamé parameters between subdomains will, therefore, not enter our bounds. Thus, we first derive a bound on the contributions, from an individual subdomain, to the different terms in (12) and we then assemble the resulting inequalities in a way very similar to how subdomain matrices are assembled into the system matrix for an entire finite element problem.

We recall that the coarse space, restricted to an individual subdomain that does not touch $\partial\Omega$, will contain all rigid body modes and that we have constructed a basis for the coarse space in terms of these modes and cutoff functions associated with the faces, edges, and vertices of the subdomain Ω_i. When constructing the coarse space component $\mathbf{u}_0$, by a specific interpolation procedure, we will make sure that all rigid body modes are reproduced and also that the remainder, $\mathbf{w}:=\mathbf{u}-\mathbf{u}_0$, will have a zero net flux across all the faces of the interface. Our construction and estimates can be used both for interior subdomains and for those with a boundary that intersects $\partial\Omega$ as our interpolation procedure will reproduce the zero Dirichlet boundary condition on $\partial\Omega_i\cap\partial\Omega$.

To assure that the zero net flux condition holds, in the almost incompressible case, we will, in a final step, introduce and estimate a face correction in terms of the remaining, independent coarse face basis functions. The correction is of the form

$$\mathbf{u}_0^{\mathrm{f}}=\sum_{ij}\beta_{ij}\theta_{\mathscr{F}^{ij}}\mathbf{n}_{\mathscr{F}^{ij}} \tag{14}$$

where the β_{ij} will be chosen so that

$$\beta_{ij}\int_{\mathscr{F}^{ij}}\theta_{\mathscr{F}^{ij}}\,\mathrm{d}A=\int_{\mathscr{F}^{ij}}(\mathbf{u}-\mathbf{u}_0^{\mathrm{v}}-\mathbf{u}_0^{\mathrm{e}})\cdot\mathbf{n}_{\mathscr{F}^{ij}}\,\mathrm{d}A \tag{15}$$

Here $\mathbf{u}_0^{\mathrm{v}}$ and $\mathbf{u}_0^{\mathrm{e}}$ are the vertex and edge components of $\mathbf{u}_0$. We then obtain $\mathbf{u}_0$ as the sum of the three terms, i.e. $\mathbf{u}_0=\mathbf{u}_0^{\mathrm{v}}+\mathbf{u}_0^{\mathrm{e}}+\mathbf{u}_0^{\mathrm{f}}$.

DOI: 10.1002/nme

The coarse interpolant $\mathbf{u}_0$ is chosen so that we can estimate $\widetilde{a}_i(\mathbf{u}-\mathbf{u}_0, \mathbf{u}-\mathbf{u}_0)$ in terms of $a_i(\mathbf{u}-\mathbf{u}_0, \mathbf{u}-\mathbf{u}_0)$, by using the following lemma, which has a constant that is uniformly bounded, for any inf–sup stable mixed finite element method, for all values of the potentially large parameters λ_i.

Lemma 3
Let $\mathbf{u}_{\text{sh}}$ denote the discrete saddle-point harmonic function with the same boundary data as $\mathbf{u}$ on $\partial\Omega_i$ and which satisfies the zero net flux condition

$$\int_{\partial\Omega_i} \mathbf{u}\cdot\mathbf{n}\,\mathrm{d}s = 0$$

Then,

$$\widetilde{a}_i(\mathbf{u}_{\text{sh}}, \mathbf{u}_{\text{sh}}) \leqslant 4\left(1+\frac{n/2}{\mu_i/\lambda_i+\beta^2}\right)\mu_i a_i(\mathbf{u},\mathbf{u}) \quad \forall \mathbf{u}\in\mathbf{V}^h \tag{16}$$

This result follows directly from [1, Lemma 3.3] by noting that a second term on the right-hand side of the inequality of that lemma vanishes in case of a zero net flux. By using this estimate, we can essentially reduce our work to issues for a compressible elasticity problem.

4.1. The coarse component of the decomposition

The construction of $\mathbf{u}_0$ begins by setting $\mathbf{u}_0(\mathcal{V}^{i\ell}) = \mathbf{u}(\mathcal{V}^{i\ell})$ at all vertices of the subdomain. While $\mathbf{u}-\mathbf{u}_0$ will vanish at all subdomain vertices, we have to estimate the contributions from the modified vertex coarse basis functions $\theta^m_{\mathcal{V}^{i\ell}}$, which differ from zero on the faces next to a vertex. We use an inverse inequality for finite element functions given in [2, Formula (4.16)]:

$$\|u_h\|^2_{L^\infty(\Omega_i)} \leqslant (C/h_i)\|u_h\|^2_{H^1(\Omega_i)}$$

to estimate the three components of $\mathbf{u}_0(\mathcal{V}^{i\ell})$, which are the coefficients for the modified coarse vertex basis functions $\theta^m_{\mathcal{V}^{i\ell}}, m=1,2,3$, in the representation of $\mathbf{u}_0^{\text{v}}$. Combining this estimate with Lemma 2, we find that with $\mathbf{u}_0^{\text{v}}$ the sum of the vertex functions of all the vertices of Ω_i,

$$|\mathbf{u}_0^{\text{v}}|^2_{\mathbf{H}^1(\Omega_i)} \leqslant C(1+\log(H_i/h_i))\|\mathbf{u}\|^2_{\mathbf{H}^1(\Omega_i)} \tag{17}$$

We also find that

$$\|\mathbf{u}_0^{\text{v}}\|^2_{\mathbf{L}^2(\mathcal{F}^{ij})} \leqslant C H_i \|\mathbf{u}\|^2_{\mathbf{H}^1(\Omega_i)} \tag{18}$$

We next recall that restrictions of the modified coarse edge basis functions to an edge are rigid body modes. We determine the coefficients for the modified coarse edge basis functions to $\mathbf{u}_0^{\text{e}}$ associated with $\mathcal{E}^{ik}$, one of the edges of $\partial\mathcal{F}^{ij}$, by solving

$$\inf_{\mathbf{r}\in\mathcal{RB}} \|I^h(\theta_{\mathcal{E}^{ik}}(\mathbf{u}-\mathbf{r}))\|^2_{\mathbf{L}^2(\mathcal{E}^{ik})} \tag{19}$$

Clearly, $\|\mathbf{u}_0^{\text{e}}\|_{\mathbf{L}^2(\mathcal{E}^{ik})} \leqslant \|\mathbf{u}\|_{\mathbf{L}^2(\mathcal{E}^{ik})} + \|I^h(\theta_{\mathcal{E}^{ik}}\mathbf{u})\|_{\mathbf{L}^2(\mathcal{E}^{ik})} \leqslant C\|\mathbf{u}\|_{\mathbf{L}^2(\mathcal{E}^{ik})}$. Given that $\|\mathbf{r}_m\|^2_{\mathbf{L}^2(\mathcal{E}^{ik})} \geqslant cH_i$, we find that the square of the coefficients of the modified coarse edge basis functions $\mathbf{u}_0^{\text{e}}$ are

DOI: 10.1002/nme

bounded by $(C/H_i)\|\mathbf{u}\|^2_{\mathbf{L}^2(\mathscr{E}^{ik})}$. By using Lemma 2, we then find that with $\mathbf{u}_0^{\mathrm{e}}$ the sum of the contributions of all the edges of Ω_i,

$$|\mathbf{u}_0^{\mathrm{e}}|^2_{\mathbf{H}^1(\Omega_i)} \leqslant C(1+\log(H_i/h_i)) \sum_k \|\mathbf{u}\|^2_{\mathbf{L}^2(\mathscr{E}^{ik})} \tag{20}$$

Here the sum is over all the edges of Ω_i. Similarly, we find that

$$\|\mathbf{u}_0^{\mathrm{e}}\|^2_{\mathbf{L}^2(\mathscr{F}^{ij})} \leqslant C H_i \sum_k \|\mathbf{u}\|^2_{\mathbf{L}^2(\mathscr{E}^{ik})}$$

In the right-hand side, we now sum over all the edges of $\partial\mathscr{F}^{ij}$.

We can estimate the right-hand sides of these two inequalities by using [2, Lemma 4.16]:

$$\|\mathbf{u}\|^2_{\mathbf{L}^2(\mathscr{E}^{ik})} \leqslant C(1+\log(H_i/h_i))\|\mathbf{u}\|^2_{\mathbf{H}^1(\Omega_i)}$$

and we obtain, by also using (17) and (20),

$$|\mathbf{u}_0^{\mathrm{v}}+\mathbf{u}_0^{\mathrm{e}}|^2_{\mathbf{H}^1(\Omega_i)} \leqslant C(1+\log(H_i/h_i))^2\|\mathbf{u}\|^2_{\mathbf{H}^1(\Omega_i)} \tag{21}$$

and similarly,

$$\|\mathbf{u}_0^{\mathrm{v}}+\mathbf{u}_0^{\mathrm{e}}\|^2_{\mathbf{L}^2(\mathscr{F}^{ij})} \leqslant C(1+\log(H_i/h_i))H_i\|\mathbf{u}\|^2_{\mathbf{H}^1(\Omega_i)} \tag{22}$$

We also have to estimate $\beta_{ij}\theta_{\mathscr{F}^{ij}}\mathbf{n}_{\mathscr{F}^{ij}}$, the correction term given in terms of the remaining independent face coarse degree of freedom on $\mathscr{F}^{ij}$. Turning to formula (15), we find that the integral on the left-hand side is of the order H_i^2, as the face $\mathscr{F}^{ij}$ has an area of that order and $\theta_{\mathscr{F}^{ij}}=1$ at all nodes of the face. By using the Cauchy–Schwarz inequality, the square of the right-hand side of (15) can be estimated by $C\|\mathbf{u}-\mathbf{u}_0^{\mathrm{v}}-\mathbf{u}_0^{\mathrm{e}}\|^2_{\mathbf{L}^2(\mathscr{F}^{ij})}H_i^2$. Thus,

$$|\beta_{ij}|^2 \leqslant C/H_i^2\|\mathbf{u}-\mathbf{u}_0^{\mathrm{v}}-\mathbf{u}_0^{\mathrm{e}}\|^2_{\mathbf{L}^2(\mathscr{F}^{ij})}$$

and by using (8), we find that

$$|\beta_{ij}\theta_{\mathscr{F}^{ij}}\mathbf{n}_{\mathscr{F}^{ij}}|^2_{\mathbf{H}^1(\Omega_i)} \leqslant C/H_i(1+\log(H_i/h_i))\|\mathbf{u}-\mathbf{u}_0^{\mathrm{v}}-\mathbf{u}_0^{\mathrm{e}}\|^2_{\mathbf{L}^2(\mathscr{F}^{ij})}$$

We can now use an elementary trace theorem, see [32, Theorem 1.2], and a scaling argument to show that

$$1/H_i\|\mathbf{u}\|^2_{\mathbf{L}^2(\mathscr{F}^{ij})} \leqslant C\|\mathbf{u}\|^2_{\mathbf{H}^1(\Omega_i)}$$

Combining this estimate with (22) and (21), we can conclude that

$$|\mathbf{u}-\mathbf{u}_0|^2_{\mathbf{H}^1(\Omega_i)} \leqslant C(1+\log(H_i/h_i))^2\|\mathbf{u}\|^2_{\mathbf{H}^1(\Omega_i)} \tag{23}$$

DOI: 10.1002/nme

We also find that

$$\|\mathbf{u}-\mathbf{u}_0\|^2_{\mathbf{L}^2(\mathscr{F}^{ij})} \leqslant C(1+\log(H_i/h_i))H_i\|\mathbf{u}\|^2_{\mathbf{H}^1(\Omega_i)} \tag{24}$$

We now consider $\widetilde{a}_i(\mathbf{u}-\mathbf{u}_0, \mathbf{u}-\mathbf{u}_0)$. As the net flux across $\partial\Omega_i$ of $\mathbf{u}-\mathbf{u}_0$ vanishes by construction, we can use Lemma 3 to obtain

$$\widetilde{a}_i(\mathbf{u}-\mathbf{u}_0, \mathbf{u}-\mathbf{u}_0) \leqslant 4\left(1+\frac{n/2}{\mu_i/\lambda_i+\beta^2}\right)\mu_i a_i(\mathbf{u}-\mathbf{u}_0, \mathbf{u}-\mathbf{u}_0)$$

By using the elementary estimate

$$a_i(\mathbf{v}, \mathbf{v}) = 2\int_{\Omega_i} \varepsilon(\mathbf{v}) : \varepsilon(\mathbf{v})\, \mathrm{d}x \leqslant 2|\mathbf{v}|^2_{\mathbf{H}^1(\Omega_i)}$$

we also have

$$\widetilde{a}_i(\mathbf{u}-\mathbf{u}_0, \mathbf{u}-\mathbf{u}_0) \leqslant 8\left(1+\frac{n/2}{\mu_i/\lambda_i+\beta^2}\right)\mu_i|\mathbf{u}-\mathbf{u}_0|^2_{\mathbf{H}^1(\Omega_i)}$$

Our recipe for $\mathbf{u}_0$ will clearly reproduce any rigid body mode. We can, therefore, replace the square of the norm on the right-hand side of (23) by $\inf_{\mathbf{r}\in\mathscr{RB}}\|\mathbf{u}-\mathbf{r}\|^2_{\mathbf{H}^1(\Omega_i)}$. We then use the following lemma:

Lemma 4
Let Ω_i be a Lipschitz domain. Then, there exists a constant $C = C(\Omega_i)$, invariant under dilation of the subdomain, such that

$$\inf_{\mathbf{r}\in\mathscr{RB}}\|\mathbf{v}-\mathbf{r}\|^2_{\mathbf{H}^1(\Omega_i)} \leqslant C a_i(\mathbf{v}, \mathbf{v})$$

This is [1, Lemma 5.2]; it is obtained by using Korn's second inequality and a Poincaré inequality. Using this result and (23), we find

$$\widetilde{a}_i(\mathbf{u}-\mathbf{u}_0, \mathbf{u}-\mathbf{u}_0) \leqslant C(1+\log(H_i/h_i))^2\mu_i a_i(\mathbf{u}, \mathbf{u})$$

We can then return to the $\widetilde{a}_i$-norm by using the elementary inequality $\mu_i a_i(\mathbf{v}, \mathbf{v}) \leqslant \widetilde{a}_i(\mathbf{v}, \mathbf{v})$.

A bound for $\widetilde{a}_i(\mathbf{u}_0, \mathbf{u}_0)$ follows from

$$\widetilde{a}_i(\mathbf{u}_0, \mathbf{u}_0) \leqslant 2\widetilde{a}_i(\mathbf{u}-\mathbf{u}_0, \mathbf{u}-\mathbf{u}_0) + 2\widetilde{a}_i(\mathbf{u}, \mathbf{u})$$

and a bound,

$$\widetilde{a}(\mathbf{u}_0, \mathbf{u}_0) \leqslant C(1+\log(H/h))^2\widetilde{a}(\mathbf{u}, \mathbf{u}) \tag{25}$$

then results by adding the contributions from all the subdomains and using the bound for the contributions from the subdomains.

4.2. The local components of the decomposition

We will now show how certain constructions and estimates provided in [1, Section 5.3] can be modified so as to find the local components $\mathbf{u}_i \in \mathbf{V}_i, i \geqslant 1$ and $\mathbf{u}_{i\delta} \in \mathbf{V}_{i\delta}$ in the decomposition of

DOI: 10.1002/nme

$\mathbf{w}=\mathbf{u}-\mathbf{u}_0$ and to complete an estimate of the parameter C_0^2 in (12). As in our previous paper, [1], we can focus on the contributions of one subdomain Ω_i and show how to partition the restriction of $\mathbf{w}$ to Ω_i. In working out our estimates, we will use the bilinear form $\widetilde{a}_i(\cdot,\cdot)$ even when deriving bounds for $\widetilde{a}_{i\delta}(\mathbf{u}_{i\delta},\mathbf{u}_{i\delta})$ in (12); we can bound this latter expression in terms of $\sum_j \widetilde{a}_j(\mathbf{u}_{i\delta},\mathbf{u}_{i\delta})$ where the sum is over all subdomains Ω_j which intersect $\Omega_{i\delta}$. Similarly, we will derive estimates in the $\mathbf{H}^1(\Omega_i)$-norm for functions that vanish outside the boundary layer subdomain $\Omega_{i\delta}$.

In our analysis, we will use alternative face and edge cutoff functions $\vartheta^{\delta}_{\mathscr{F}^{ij}}$ and $\vartheta^{\delta}_{\mathscr{E}^{ik}}$, introduced in [1, Section 5.3], which are supported in the closure of $\Omega_{i\delta}$. Together with the nodal basis functions for the subdomain vertices, they provide a partition of unity on Γ_i.

For each face $\mathscr{F}^{ij}$ of Ω_i, we consider the intersection $\Omega_{i\delta}\cap\Omega_{j\delta}\cap\Omega_i$. The alternative face cutoff function, $\vartheta^{\delta}_{\mathscr{F}^{ij}}$, is supported in the closure of this set and satisfies the following bounds:

$$|I^h(\vartheta^{\delta}_{\mathscr{F}^{ij}}\mathbf{u})|^2_{\mathbf{H}^1(\Omega_i)}\leqslant C(H_i/\delta_i)(1+\log(H_i/\delta_i))(1+\log(H_i/h_i))\|\mathbf{u}\|^2_{\mathbf{H}^1(\Omega_i)} \tag{26}$$

and

$$|I^h(\vartheta^{\delta}_{\mathscr{F}^{ij}}\mathbf{r}_m)|^2_{\mathbf{H}^1(\Omega_i)}\leqslant C(H_i/\delta_i)(1+\log(H_i/\delta_i))H_i,\quad m=1,\ldots,6 \tag{27}$$

see [1, Lemma 5.4].

We can now provide a bound for $|I^h(\vartheta^{\delta}_{\mathscr{F}^{ij}}\mathbf{w})|^2_{\mathbf{H}^1(\Omega_i)}$. We do so by writing $\mathbf{w}=\mathbf{u}-\mathbf{u}_0$ and by first using (26) to estimate the norm of $I^h(\vartheta^{\delta}_{\mathscr{F}^{ij}}\mathbf{u})$. We next note that $I^h(\vartheta^{\delta}_{\mathscr{F}^{ij}}\theta_{\mathscr{F}^{ij}}\mathbf{r}_k)=I^h(\vartheta^{\delta}_{\mathscr{F}^{ij}}\mathbf{r}_k)$ on Γ_i. Therefore, we can use (27) and the bound for the square of the coefficients of $I^h(\theta_{\mathscr{F}^{ij}}\mathbf{r}_k)$ in the representation of $\mathbf{u}_0$ to bound $I^h(\vartheta^{\delta}_{\mathscr{F}^{ij}}\mathbf{u}_0)$. We recall from Section 4.1 that there are three types of contributions to that coefficient and that the square of all of them are bounded by

$$C/H_i(1+\log(H_i/h_i))\|\mathbf{u}\|^2_{\mathbf{H}^1(\Omega_i)} \tag{28}$$

We can therefore obtain

$$|I^h(\vartheta^{\delta}_{\mathscr{F}^{ij}}\mathbf{w})|^2_{\mathbf{H}^1(\Omega_i)}\leqslant C(H_i/\delta_i)(1+\log(H_i/\delta_i))(1+\log(H_i/h_i))\|\mathbf{u}\|^2_{\mathbf{H}^1(\Omega_i)}$$

The alternative edge cutoff function, $\vartheta^{\delta}_{\mathscr{E}^{ik}}$, is supported in the closure of the intersection of the $\Omega_{j\delta}$ that contains the edge $\mathscr{E}^{ik}$. We have the following bounds:

$$|I^h(\vartheta^{\delta}_{\mathscr{E}^{ik}}\mathbf{u})|^2_{\mathbf{H}^1(\Omega_i)}\leqslant C(1+\log(H_i/h_i))\|\mathbf{u}\|^2_{\mathbf{H}^1(\Omega_i)} \tag{29}$$

and

$$|I^h(\vartheta^{\delta}_{\mathscr{E}^{ik}}\mathbf{r}_m)|^2_{\mathbf{H}^1(\Omega_i)}\leqslant C H_i,\quad m=1,\ldots,6 \tag{30}$$

see [1, Lemma 5.5]. We can use (29) directly and what remains is to estimate the norm of $I^h(\vartheta^{\delta}_{\mathscr{E}^{ik}}\mathbf{u}_0)$. We partition this function by using $\theta_{\mathscr{F}^{ij}}$, $\theta_{\mathscr{F}^{i\ell}}$, and $\theta_{\mathscr{E}^{ik}}$, where $\mathscr{F}^{i\ell}$ is the other face of Ω_i with $\mathscr{E}^{ik}$ a part of its boundary. The estimate for the coefficients of the face contributions, (28), plays the same role as before. In addition, we can bound the norm of $I^h(\theta_{\mathscr{F}^{ij}}\vartheta^{\delta}_{\mathscr{E}^{ik}})$ in the same way as in (8) resulting in a bound with a factor $(1+\log(H_i/h_i))^2$. For the edge contribution,

DOI: 10.1002/nme

$I^h(\theta_{\mathscr{E}^{ik}}\vartheta^{\delta}_{\mathscr{E}^{ik}}\mathbf{u}_0)$, we note that $I^h(\theta_{\mathscr{E}^{ik}}\vartheta^{\delta}_{\mathscr{E}^{ik}})=\theta_{\mathscr{E}^{ik}}$. The coefficient for this term can then be estimated by $\|\mathbf{u}\|_{\mathbf{L}^2(\mathscr{E}^{ik})}$ and we find,

$$|I^h(\vartheta^{\delta}_{\mathscr{E}^{ik}}\mathbf{u}_0)|^2_{\mathbf{H}^1(\Omega_i)}\leqslant C(1+\log(H_i/h_i))^2\|\mathbf{u}\|^2_{\mathbf{H}^1(\Omega_i)}$$

We also have to estimate certain correction terms as in [1, (5.18)]; their purpose is to create face and edge contributions that individually have no net flux. There are no new difficulties in obtaining a bound consistent with that of Theorem 1; in this work we can use (24). As in [1, Section 5.3] a function $\mathbf{w}_{\mathscr{F}^{ij}}$ can be constructed, which satisfies the no net flux condition across the face $\mathscr{F}^{ij}$ and vanishes on the interface Γ outside this face. We then allocate $(\frac{1}{2})\mathbf{w}_{\mathscr{F}^{ij}}$ to each of $\mathbf{u}_i\in\mathbf{V}_{i\delta}$ and $\mathbf{u}_j\in\mathbf{V}_{j\delta}$ and we can then use a bound similar to one established in [1]:

$$\widetilde{a}_i(\mathbf{w}_{\mathscr{F}^{ij}},\mathbf{w}_{\mathscr{F}^{ij}})\leqslant C(H_i/\delta_i)^3(1+\log(H_i/h_i))^2\widetilde{a}_i(\mathbf{u},\mathbf{u}) \tag{31}$$

For the components of $\mathbf{w}$ associated with the subdomain edge $\mathscr{E}^{ik}$, we can proceed as in [1] and construct a function $\mathbf{w}_{\mathscr{E}^{ik}}$, with zero net flux. This function, for which there is a bound of the same quality as (31), then contributes, in equal part, to the elements $\mathbf{u}_{j\delta}\in V_{j\delta}$ of (12) for the $\Omega_{j\delta}$ that contain that edge. We note that this construction provides elements in the subspaces $V_{j\delta}$ that are continuous if the same recipes are used in all subdomains Ω_j.

The sum of these face and edge functions for the subdomain Ω_i equals $\mathbf{w}$ on $\partial\Omega_i$; we recall that $\mathbf{w}$ vanishes at the subdomain vertices. We can, therefore, choose as $\mathbf{u}_i\in\mathbf{V}_i$, in the decomposition of $\mathbf{w}$, what remains of $\mathbf{w}$ after all these face and edge functions have been subtracted from it. We can then find a bound of the same quality for $\widetilde{a}_i(\mathbf{u}_i,\mathbf{u}_i)$ as for the contributions to the other local subspaces by using the triangular inequality.

Combining the resulting estimates with the estimate of $\widetilde{a}(\mathbf{u}_0,\mathbf{u}_0)$, as given in (25), we have a bound for C_0^2, and have thus completed the proof of the lower bound for the Schwarz operator P_{hyb}, and the proof of Theorem 1.

4.3. The compressible elasticity case

The proof of Theorem 2 essentially only requires arguments that have been used previously to analyze Schwarz methods based on overlapping subdomains; see, e.g. [2, Chapter 3]. A variant of these arguments are used in [16] in which the older theory is extended to the case with large variations of the coefficients across the interface. We note that the logarithmic factor in Theorem 2 originates from the bound for $\mathbf{u}_0$.

We also note that we can establish the same result as in Theorem 1 in case we use a conventional finite element model for subdomains, where the material is compressible, and a mixed finite element method for those that are almost incompressible. All that is required is that the finite element meshes and degrees of freedom match across the interface and that we use an extra independent coarse face degree of freedom as in (14) for each face of the subdomains that are almost incompressible.

5. NUMERICAL RESULTS

Results are presented in this section to confirm the theory and to demonstrate the usefulness of our algorithm. Attention is restricted primarily to meshes of inf–sup stable Q_2-P_1 hexahedral elements, but we also consider lower-order Q_1-P_0 elements in some cases. The Q_1-P_0 element

DOI: 10.1002/nme

is not inf–sup stable and could have convergence issues for Poisson ratios close to $\frac{1}{2}$, but it is often used in practice for reasons of convenience. We note that it is equivalent to a standard displacement-based Q_1 elasticity element with selective reduced integration of bulk strain energy; see, e.g. [33, Section 4.4]. Pressure unknowns can be eliminated at the element level for both $Q_2 - P_1$ and $Q_1 - P_0$ if the Poisson ratio is less than $\frac{1}{2}$.

Unless specified otherwise, the results presented are for linear systems of equations with random right-hand sides solved to a relative residual tolerance of 10^{-8} using the conjugate gradient method. Iteration counts and condition number estimates of the preconditioned operator are denoted by iter. and cond., respectively, in the tables.

Selected results are also presented for two variants of the preconditioner. Variant 1 uses a multiplicative coarse correction rather than an additive one; see, e.g. [25, Section 3.2.1]. In this case, the Schwarz method is based on the polynomial

$$P_{v1} = (I - P_0)\left(I - \sum_{i=1}^{N} P_i\right)\left(\sum_{i=1}^{N} P_{i\delta}\right)\left(I - \sum_{i=1}^{N} P_i\right)(I - P_0)$$

Comparing P_{v1} with P_{hyb}, we see that the coarse correction is now applied in the first and final step. In practice, however, it is only necessary to apply the coarse correction once for each iteration after an initialization step. Variant 2 is identical to Variant 1 with the exception that $P_{i\delta}$ in the expression above for P_{v1} is replaced by

$$P_{iw\delta} = R_{i\delta}^{\mathrm{T}} \widetilde{P}_{iw\delta} \quad \text{with } \widetilde{P}_{iw\delta} \text{ defined by } \widetilde{a}_{id}(\widetilde{P}_{iw\delta}\mathbf{u}, \mathbf{v}) = \widetilde{a}(\mathbf{u}, R_{id}^{\mathrm{T}} D^{-1}\mathbf{v}) \quad \forall \mathbf{v} \in \mathbf{V}_{i\delta}$$

where D is a diagonal matrix; the value of $\mathbf{v}$ at a node is divided by the number of boundary layer subdomains to which it belongs. Variant 2 basically scales right-hand sides prior to applying local solvers. This results in a nonsymmetric preconditioner, and thus the standard conjugate gradient algorithm can no longer be used. Nevertheless, by using a Krylov method that minimizes the energy of the error, just as conjugate gradients does, we find that the number of iterations can be reduced significantly. A related preconditioning strategy is described in [34, Remark 2.7]. We note that we can prove the same bounds for the Schwarz method based on P_{v1} as for P_{hyb}, but that we do not know how to analyze Variant 2. We also note that the range of these two variants of the original hybrid operator also belongs to the space of discrete saddle-point harmonic functions.

We present results for incompressible elasticity in the final example even though our theory does not apply directly to this case; a more thorough treatment will appear elsewhere. It is no longer possible to eliminate pressure unknowns at the element level, and we augment the coarse space with a constant pressure for each subdomain. Thus, the coarse space dimension increases by the number of subdomains, and the coarse problem is a saddle-point system rather than a positive definite one. Right preconditioned GMRES [35, Section 9.3.2] is used as the Krylov subspace method.

5.1. Example 1

The first example is for a unit cube domain decomposed into 64 smaller cube subdomains as shown in Figure 1. Here we use $Q_2 - P_1$ elements, and include a single layer of elements on either side of subdomain boundaries for the boundary layer subdomains (see Figure 1 right). The Poisson ratio

DOI: 10.1002/nme

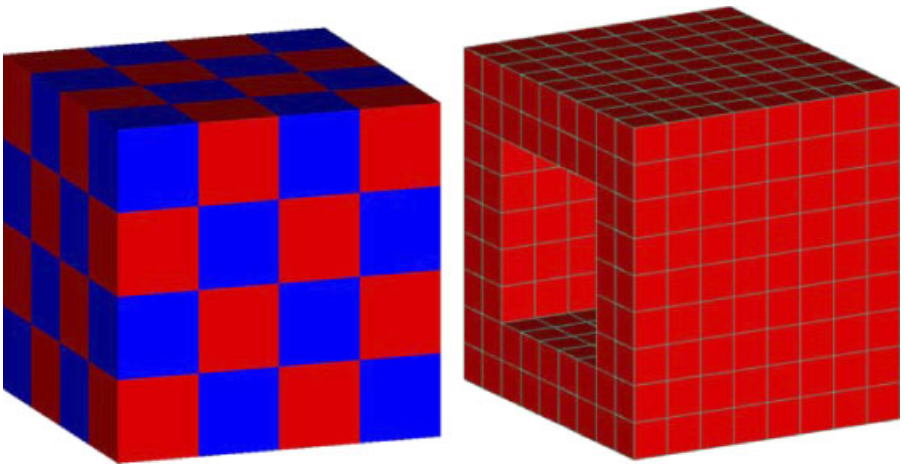

Figure 1. Domain decomposition of cube domain for Example 1 (left) and an example boundary layer subdomain taken from the left side of the cube and magnified (right).

ν is the same in each of the subdomains, and Young's modulus E equals σ in the light subdomains and 1 in the dark subdomains. We note for $\sigma \neq 1$ that this checkerboard distribution of material properties is not quasi-monotone, cf. [36]. Results with essential boundary conditions, on different subsets of the boundary $\partial\Omega$, are given in Table I.

The results in Table I exhibit similar trends whether all six sides of the cube are constrained or just one. For values of ν not too close to the incompressible limit of $\frac{1}{2}$, the coarse spaces with and without an independent degree of freedom for each subdomain face lead to very similar results. In contrast, results are insensitive to changes in ν near $\frac{1}{2}$ only for the coarse space that includes independent face degrees of freedom. We also see that the results are fairly insensitive to jumps in the material property σ as predicted by theory.

5.2. *Example 2*

We now fix $\nu = 0.3$ in the previous example, and vary the ratio H/h while keeping the overlap ratio $H/\delta = 4$ fixed. In addition, $Q_1 - P_0$ elements are used instead of $Q_2 - P_1$ elements in order to allow us to confirm a condition number estimate for larger values of H/h. Results are shown in Table II for the coarse space based on corners and edges only ($c+e$) and the richer coarse space of [1] based on corners, edges, and faces ($c+e+f$). A logarithmic plot of these results in Figure 2 suggests for the $c+e$ coarse space that the exponent p of the factor $(1+\log(H/h))^p$ in the condition number estimate is not greater than 2 for both $\sigma = 1$ and $\sigma = 100$. Indeed, for $\sigma = 1$ we observe $p \approx 1$ and p is only slightly greater than 1 for $\sigma = 100$. These results suggest that it may be possible to reduce p from 2 to 1 in our current theory, at least, for quasi-monotone coefficient distributions. Consistent with the theory for the unreduced coarse space [1], the exponent p appears to be bounded above by 1 for $c+e+f$ for both values of σ; we note that a factor in the bound in [1] has been improved from $(1+\log(H/h))^2$ to $(1+\log(H/h))(1+\log(H/\delta))$ in the final version of that paper.

DOI: 10.1002/nme

Table I. Example 1 results for $H/h=7$ and $H/\delta=7$. The number of unknowns, the Poisson ratio, and the number of coarse degrees of freedom are denoted by ndof, ν, and ncdof, respectively.

	All sides constrained, ndof = 499, 125						Left side only constrained, ndof = 545, 832					
	$\sigma=1$		$\sigma=100$		$\sigma=10000$		$\sigma=1$		$\sigma=100$		$\sigma=10000$	
ν	Iter.	Cond.	Iter.	Cond.	Iter.	Cond.	Iter.	Cond.	Iter.	Cond.	Iter.	Cond.
Corners + edges + face bubble for coarse space, ncdof = 765												
0.3	38	19.6	56	35.3	57	38.0	51	25.4	87	74.0	95	98.3
0.4	42	20.6	59	38.6	61	41.6	53	27.5	93	79.8	100	104
0.49	49	30.5	70	53.3	74	58.2	63	35.7	109	105	115	128
0.499	50	35.3	71	60.9	77	65.7	67	39.3	113	116	121	139
0.4999	52	37.3	70	65.5	77	66.4	68	40.4	115	120	123	147
Corners + edges only for coarse space, ncdof = 621												
0.3	40	20.3	62	48.9	64	53.4	52	26.8	118	125	131	171
0.4	44	22.9	68	56.8	70	62.8	56	29.2	128	143	141	191
0.49	66	60.7	91	103	104	136	82	63.9	162	232	181	281
0.499	82	113	107	153	123	205	101	110	181	284	211	471
0.4999	88	132	113	186	126	183	108	124	190	313	217	432

DOI: 10.1002/nme

Table II. Example 2 results for $\nu=0.3$, $H/\delta=4$, and the left side only constrained.

		$\sigma=1$				$\sigma=100$			
		$c+e+f$		$c+e$		$c+e+f$		$c+e$	
H/h	ndof	Iter.	Cond.	Iter.	Cond.	Iter.	Cond.	Iter.	Cond.
4	13 872	31	13.5	37	15.9	35	15.0	71	55.0
8	104 544	39	17.6	43	19.9	45	19.5	88	72.2
12	345 744	42	19.9	45	22.3	49	22.1	91	84.2
16	811 200	44	21.5	47	24.0	51	23.9	95	93.1
20	1574 640	46	22.7	49	25.4	53	25.2	100	100
24	2 709 792	47	23.7	50	26.4	55	26.2	104	106

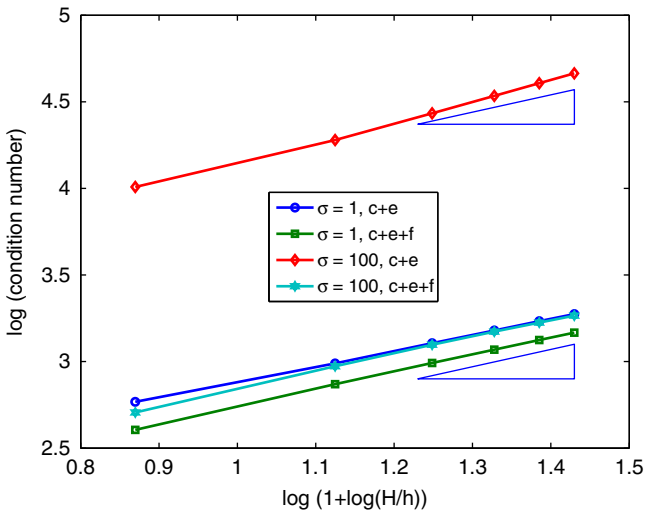

Figure 2. Logarithmic plot of Table II data. The two triangles in the figure have unit slopes.

5.3. *Example 3*

The next example is used to demonstrate the scalability of our algorithm with respect to the number of subdomains. Here again, we consider a unit cube decomposed into smaller cubic subdomains having $H/h=7$ and $H/\delta=7$, but now both E and ν are constant. The results in Table III show that only the coarse space with face degrees of freedom leads to a scalable algorithm as ν approaches $\frac{1}{2}$. Both coarse spaces, however, are scalable for values of ν not too close to $\frac{1}{2}$.

5.4. *Example 4*

In the fourth example, we fix $H/h=12$ and vary H/δ for a unit cube domain decomposed into 64 smaller cube subdomains. We see in Table IV a much stronger dependence on the overlap parameter H/δ for values of ν near $\frac{1}{2}$ as predicted by theory.

DOI: 10.1002/nme

Table III. Example 3 results for N subdomains with $H/h=7$ and $H/\delta=7$.

		Poisson ratio $\nu=0.3$				Poisson ratio $\nu=0.4999$			
		$c+e+b$		$c+e$		$c+e+b$		$c+e$	
N	ndof	Iter.	Cond.	Iter.	Cond.	Iter.	Cond.	Iter.	Cond.
8	59 049	28	12.7	28	14.8	50	45.6	62	227
27	206 763	35	17.0	37	19.0	51	37.7	77	106
64	499 125	38	19.6	40	20.3	52	37.3	88	132
125	985 527	42	21.1	41	21.7	52	38.3	94	148
216	1 715 361	43	22.1	44	22.6	53	39.1	98	158
343	2 738 019	45	22.9	46	23.3	53	39.6	100	162
512	4 102 893	46	23.5	46	23.8	53	39.9	102	169

The coarse space based on corners and edges only is designated by $c+e$, while $c+e+b$ denotes the same coarse space augmented with a single degree of freedom for each subdomain face. All six sides of the domain are constrained.

Table IV. Example 4 results for 64 subdomains with $H/h=12$.

	$\nu=0.3$		$\nu=0.499$	
H/δ	Iter.	Cond.	Iter.	Cond.
3	46	23.0	62	35.5
4	49	25.4	65	38.7
6	54	28.2	73	44.0
12	61	33.0	120	136

The left side of the domain is fixed and there are 1 196 712 unknowns. The coarse space includes corners, edges, and one degree of freedom for each subdomain face.

5.5. *Example 5*

Here we consider the two meshes and mesh decompositions shown in Figures 3 and 4. The material properties are constant throughout the structure in Figure 3, while those for the structure in Figure 4 vary as described in the caption. Notice for the decomposition of Mesh 2 that material properties are not constant in each subdomain. Although our theory does not cover this important case, the algorithm appears to perform well for this problem. The theory does not apply to the Mesh 1 problem with constant material properties because it has irregular-shaped subdomains. We also note that the theory does not apply for meshes of Q_1-P_0 elements if ν is close to $\frac{1}{2}$ because this element is not inf–sup stable. Nevertheless, we observe in Table V satisfactory performance of our algorithm in this case as well. Variants 1 and 2 of the preconditioner both lead to noticeable reductions in iteration counts over all values of the Poisson ratio for meshes of Q_2-P_1 elements. The same does not necessarily hold for meshes of Q_1-P_0 elements near the incompressible limit. The mesh decompositions for this example were obtained using a tool based on the graph partitioning program Chaco [37].

5.6. *Example 6*

With reference to Examples 1 and 3, we now investigate the scalability of our method for the incompressible case of $\nu=\frac{1}{2}$. In contrast to the previous examples, we do not eliminate displacement and pressure unknowns in subdomain interiors. Moreover, we use standard overlapping subdomains,

DOI: 10.1002/nme

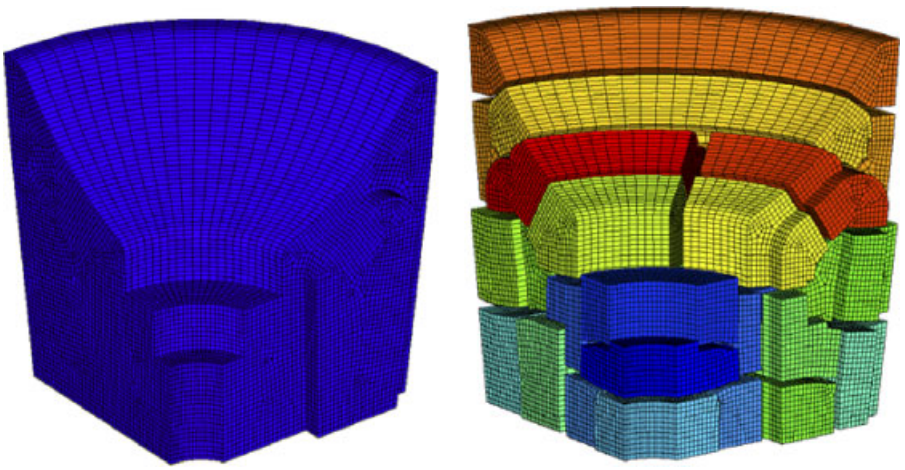

Figure 3. Mesh 1 for Example 5 and decomposition into 20 subdomains. Young's modulus and the Poisson ratio are constant with $E = 10e6$ and ν given in Table V. All three degrees of freedom of nodes at the bottom of the mesh are fixed.

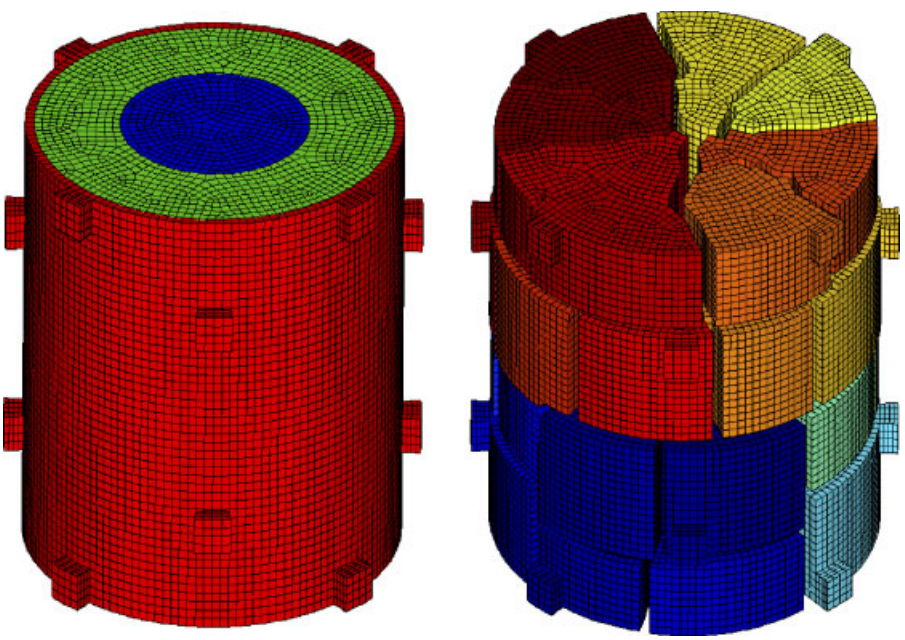

Figure 4. Mesh 2 for Example 5 and decomposition into 40 subdomains. The material properties in the inner(1), middle(2), and outer(3) cylindrical regions (see left figure) are $(E_1, E_2, E_3) = (30e6, 15e6, 10e6)$ and $(\nu_1, \nu_2, \nu_3) = (0.3, \nu, 0.33)$, where ν is given in Table V. All three degrees of freedom of nodes at the bottom of the mesh are fixed.

DOI: 10.1002/nme

Table V. Example 5 results for meshes and decompositions shown in Figures 3 and 4. M^{-1} denotes the subject preconditioner of this study, while M_{v1}^{-1} and M_{v2}^{-1} are the two variants described at the beginning of this section. The coarse space includes the additional degree of freedom for each subdomain face, and two layers of elements on either side of subdomain boundaries are used for the boundary layer (overlap) subdomains.

	Q_2-P_1, ndof = 1 196 712					Q_1-P_0, ndof = 155 106				
	M^{-1}		M_{v1}^{-1}		M_{v2}^{-1}	M^{-1}		M_{v1}^{-1}		M_{v2}^{-1}
v	Iter.	Cond.	Iter.	Cond.	Iter.	Iter.	Cond.	Iter.	Cond.	Iter.
Mesh 1 results for 20 subdomains										
0.3	87	159	79	137	48	87	153	73	120	51
0.4	97	199	88	171	57	96	196	82	153	59
0.49	143	520	137	444	92	156	581	136	437	105
0.499	175	867	165	711	112	206	1.13e3	184	821	159
0.4999	182	954	175	778	117	228	1.32e3	200	929	287
Mesh 2 results for 40 subdomains										
	Q_2-P_1, ndof = 2 046 528					Q_1-P_0, ndof = 261 888				
0.3	59	29.8	42	16.9	23	50	21.9	36	13.2	21
0.4	61	32.4	47	21.6	26	53	24.2	40	16.8	24
0.49	77	55.6	61	41.8	36	67	41.7	53	31.8	34
0.499	84	66.2	67	49.9	39	75	48.3	59	38.1	41
0.4999	85	69.8	69	52.8	40	88	55.5	78	51.5	54

Table VI. Incompressible elasticity results (iterations) for structured mesh decompositions with $H/h=7$ and $H/\delta=7$. All six faces of the cube domain are constrained, and the coarse space includes the additional degree of freedom for each subdomain face.

		$\sigma=1$			$\sigma=100$		
N	ndof	M^{-1}	M_{v1}^{-1}	M_{v2}^{-1}	M^{-1}	M_{v1}^{-1}	M_{v2}^{-1}
8	70 025	41	41	25	37	32	23
27	243 807	48	43	33	51	38	30
64	586 933	50	44	35	60	39	34
125	1 157 027	51	45	36	62	40	35
216	2 011 713	52	44	36	64	40	36
343	3 208 615	52	44	36	65	40	37
512	4 805 357	52	44	37	65	40	37

as in [1], rather than the boundary layer subdomains. As was true for compressible and almost incompressible cases, it is apparent in Table VI that the method has very good scalability with respect to the number of subdomains. Condition number estimates are not provided in Table VI because GMRES was used rather than conjugate gradients for this example.

REFERENCES

1. Dohrmann CR, Widlund OB. An overlapping Schwarz algorithm for almost incompressible elasticity. *SIAM Journal on Numerical Analysis* 2009; **47**(4):2897–2923. Available from: http://www.cs.nyu.edu/cs/faculty/widlund/AIErev.pdf.

DOI: 10.1002/nme

2. Toselli A, Widlund O. *Domain Decomposition Methods—Algorithms and Theory*. Springer Series in Computational Mathematics, vol. 34. Springer: Berlin, Heidelberg, New York, 2005.
3. Dryja M, Smith BF, Widlund OB. Schwarz analysis of iterative substructuring algorithms for elliptic problems in three dimensions. *SIAM Journal on Numerical Analysis* 1994; **31**(6):1662–1694.
4. Dohrmann CR, Klawonn A, Widlund OB. A family of energy minimizing coarse spaces for overlapping Schwarz preconditioners. In *Proceedings of the 17th International Conference on Domain Decomposition Methods in Science and Engineering*, Langer U, Discacciati M, Keyes D, Widlund O, Zulehner W (eds), Strobl, Austria, 3–7 July 2006. Lecture Notes in Computational Science and Engineering, vol. 60. Springer: Berlin, 2007; 247–254.
5. Bhardwaj M, Reese G, Driessen B, Alvin K, Day D. Salinas—an implicit finite element structural dynamics code developed for massively parallel platforms. *Forty-first AIAA/ASME/ASCE/AHS/ASC SDM*, Atlanta, GA, 3–6 April 2000. *AIAA 2000-1651*, 2000.
6. Smith BF. An optimal domain decomposition preconditioner for the finite element solution of linear elasticity problems. *SIAM Journal on Scientific and Statistical Computing* 1992; **13**(1):364–378.
7. Smith BF. Domain decomposition algorithms for the partial differential equations of linear elasticity. *Ph.D. Thesis*, Courant Institute of Mathematical Sciences, September 1990. *Technical Report 517*, Department of Computer Science, Courant Institute.
8. Klawonn A, Pavarino LF. Overlapping Schwarz methods for mixed linear elasticity and Stokes problems. *Computer Methods in Applied Mechanics and Engineering* 1998; **165**:233–245.
9. Klawonn A, Pavarino LF. A comparison of overlapping Schwarz methods and block preconditioners for saddle point problems. *Numerical Linear Algebra with Applications* 2000; **7**:1–25.
10. Dohrmann CR. Preconditioning of saddle point systems by substructuring and a penalty approach. In *Domain Decomposition Methods in Sciences and Engineering XVI*, Keyes DE, Widlund OB (eds). Lecture Notes in Computational Science and Engineering, vol. 55. Springer: Berlin, 2006; 53–64. *Proceedings of the 16th International Conference on Domain Decomposition Methods*, New York City, 11–15 January 2005.
11. Goldfeld P, Pavarino LF, Widlund OB. Balancing Neumann–Neumann preconditioners for mixed approximations of heterogeneous problems in linear elasticity. *Numerische Mathematik* 2003; **95**(2):283–324.
12. Li J. A dual–primal FETI method for incompressible Stokes equations. *Numerische Mathematik* 2005; **102**: 257–275.
13. Li J, Widlund OB. BDDC algorithms for incompressible Stokes equations. *SIAM Journal on Numerical Analysis* 2006; **44**(6):2432–2455.
14. Brezzi F, Fortin M. *Mixed and Hybrid Finite Element Methods*. Springer: Berlin, 1991.
15. Brenner SC, Scott R. *The Mathematical Theory of Finite Element Methods* (3rd edn). Springer: Berlin, Heidelberg, New York, 2008.
16. Dohrmann CR, Klawonn A, Widlund OB. Domain decomposition for less regular subdomains: overlapping Schwarz in two dimensions. *SIAM Journal on Numerical Analysis* 2008; **46**(4):2153–2168.
17. Klawonn A, Rheinbach O, Widlund OB. An analysis of a FETI–DP algorithm on irregular subdomains in the plane. *SIAM Journal on Numerical Analysis* 2008; **46**(5):2484–2504.
18. Boffi D, Gastaldi L. On the quadrilateral $Q_2 - P_1$ element for the Stokes problem. *International Journal for Numerical Methods in Fluids* 2002; **39**(11):1001–1011.
19. Paz RR, Nigro NM, Storti MA. On the efficiency and quality of numerical solutions in CFD problems using the interface strip preconditioner for domain decomposition methods. *International Journal for Numerical Methods in Fluids* 2006; **52**(1):89–118.
20. Quarteroni A, Sala M, Valli A. An interface-strip domain decomposition preconditioner. *SIAM Journal on Scientific Computing* 2006; **28**(2):498–516.
21. Dohrmann CR. A preconditioner for substructuring based on constrained energy minimization. *SIAM Journal on Scientific Computing* 2003; **25**(1):246–258.
22. Klawonn A, Rheinbach O. Robust FETI-DP methods for heterogeneous three dimensional linear elasticity problems. *Computer Methods in Applied Mechanics and Engineering* 2007; **196**(8):1400–1414.
23. Klawonn A, Widlund OB. Dual–primal FETI methods for linear elasticity. *Communications on Pure and Applied Mathematics* 2006; **59**(11):1523–1572.
24. Mandel J. Iterative solvers by substructuring for the p-version finite element method. *Computer Methods in Applied Mechanics and Engineering* 1990; **80**:117–128.
25. Smith BF, Bjørstad P, Gropp W. *Domain Decomposition*: *Parallel Multilevel Methods for Elliptic Partial Differential Equations*. Cambridge University Press: New York, 1996.

DOI: 10.1002/nme

26. Pavarino LF, Widlund OB. Iterative substructuring methods for spectral element discretizations of elliptic systems. I. Compressible linear elasticity. *SIAM Journal on Numerical Analysis* 2000; **37**(2):353–374.
27. Bramble JH, Pasciak JE, Schatz AH. The construction of preconditioners for elliptic problems by substructuring. IV. *Mathematics of Computation* 1989; **53**(187):1–24.
28. Smith BF. A domain decomposition algorithm for elliptic problems in three dimensions. *Numerische Mathematik* 1991; **60**(2):219–234.
29. Pearson K. On lines and planes of closest fit to systems of points in space. *Philosophical Magazine* 1901; **26**:559–572.
30. Mandel J, Brezina M. Balancing domain decomposition for problems with large jumps in coefficients. *Mathematics of Computation* 1996; **65**(216):1387–1401.
31. Mandel J. Hybrid domain decomposition with unstructured subdomains. In *Domain Decomposition Methods in Science and Engineering*, *Sixth International Conference of Domain Decomposition*, Mandel J, Farhat C, Cai XC (eds), Como, Italy, 15–19 June 1992. AMS Contemporary Mathematics, vol. 157. 1994; 103–112.
32. Nečas J. *Les Méthodes Directes en Théorie des Équations Elliptiques*. Academia: Prague, 1967.
33. Hughes TJ. *The Finite Element Method*: *Linear Static and Dynamic Finite Element Analysis*. Prentice-Hall: Englewood Cliffs, NJ, 1987.
34. Cai XC, Sarkis M. Timely communication: a restricted additive Schwarz preconditioner for general sparse linear systems. *SIAM Journal on Scientific Computing* 1999; **21**(2):792–797.
35. Saad Y. *Iterative Methods for Sparse Linear Systems*. SIAM: Philadelphia, PA, 2003.
36. Dryja M, Sarkis MV, Widlund OB. Multilevel Schwarz methods for elliptic problems with discontinuous coefficients in three dimensions. *Numerische Mathematik* 1996; **72**:313–348.
37. Hendrickson B, Leland R. The Chaco user's guide, version 2.0. *Technical Report SAND94-2692*, Sandia National Laboratories, 1994.

DOI: 10.1002/nme